Applied Physics Letters ARTICLE scitation.org/journal/apl

Nondestructive evaluation of structural adhesive bonding using the attenuation of zero-group-velocity Lamb modes

Cite as: Appl. Phys. Lett. **116**, 104101 (2020); doi: 10.1063/1.5143215
Submitted: 20 December 2019 · Accepted: 25 February 2020 ·
Published Online: 9 March 2020

R. Hodé,[1,2,a] S. Raetz,[1,b] J. Blondeau,[1] N. Chigarev,[1] N. Cuvillier,[2] V. Tournat,[1] and M. Ducousso[2,c]

AFFILIATIONS

[1]Laboratoire d'Acoustique de l'Université du Mans, LAUM–UMR 6613 CNRS, Le Mans Université, Avenue O. Messiaen, 72085 Le Mans Cedex 9, France
[2]Safran Tech, Rue des Jeunes Bois, Châteaufort, 78772 Magny-les-Hameaux, France

[a]Author to whom correspondence should be addressed: romainod@gmail.com
[b]Electronic mail: samuel.raetz@univ-lemans.fr
[c]Electronic mail: mathieu.ducousso@safrangroup.com

ABSTRACT

A laser ultrasonic method is proposed for the nondestructive evaluation (NDE) of structural adhesive bonding. Zero-group-velocity (ZGV) resonances were generated and detected in five trilayer assemblies composed of two asymmetric aluminum alloy plates bonded with an epoxy adhesive. Cohesive and adhesive defects were introduced to degrade the practical adhesion. The attenuation of the temporal signal of ZGV resonances was found to provide sufficient information to discriminate between strong and weak bonding. Two metrics characterizing the attenuation were identified, which allow us to quantitatively evaluate the differences between the manufactured samples. A 2D scan of a trilayer assembly with different bond defects demonstrates the imaging capability of this all-optical NDE method.

Structural adhesive bonding is important in aeronautics. Indeed, this assembly technique has numerous benefits compared to conventional techniques like riveting or welding. It allows lighter aircraft structures and is one of the best ways to join composite materials, which meet the needs of a high strength-to-weight ratio. Nevertheless, wider deployment of this assembly technique is hampered by the absence of a nondestructive method[1–4] to certify the practical adhesion.

In industrial applications, bonded assemblies must withstand a mechanical load that is defined by the manufacturer. In the following, if this level is satisfied, the bonding will be qualified as strong, and if not, as weak. However, even for weak bonding, the adhesion is not null in practice. Thus, it is difficult for a nondestructive evaluation (NDE) to differentiate between weak and strong bonding. In the literature, a large number of NDE methods have been investigated to qualitatively or quantitatively evaluate the mechanical strength (practical adhesion) of bonded assemblies.

One of the most promising quantitative techniques is based on laser-generated shock waves, often referred to as a laser shock adhesion test (LASAT).[5] In this method, a high dynamical and mechanical tensile stress is applied to a bonded joint with shock waves. Ducousso *et al.*[6] succeeded in quantifying the practical adhesion of a trilayer bonded assembly (TA6V4 titanium alloy/epoxy/3D-woven composite) thanks to this method. One identified limitation of this technique, notably highlighted by Ehrhart *et al.*,[7] is that the process must be thoughtfully calibrated so that other parts of the structure are not degraded by the propagation of the shock waves. Ultrasonic techniques, which are absolutely nondestructive, have not yet been developed to overcome this potential limitation of LASAT in quantifying bonded assemblies.

Of the nondestructive ultrasonic techniques, various approaches based on the reflection[8–11] or transmission[12,13] of bulk waves at imperfect interfaces have been proposed. These methods are highly sensitive to a strong impedance mismatch, which allows one to detect voids or disbonds. However, the small impedance differences between strong and weak bonds make the detection of imperfect interfaces difficult. Thus, accurate post-processing methods have been developed to identify the key metrics that characterize the mechanical strength of adhesive bonding.[8–13] To name a few, other ultrasonic methods based on non-linear phenomena of bulk waves[14] or on measuring guided

waves[15–19] allow one to obtain an average value for the practical adhesion along a joint. To achieve better defect localization, zero-group-velocity (ZGV) Lamb modes[20,21] have been studied.[22–25] Mezil *et al.*[26] carried out theoretical and experimental investigations of a symmetrical trilayer composed of two duralumin plates bonded with an epoxy adhesive. They found that the frequencies of the ZGV modes are sensitive to the quality of the bonding. Thus, these ZGV modes are good candidates for nondestructively evaluating the interfacial stiffnesses that model the mechanical coupling between the bonded layers. These local resonances can be applied in a wider context for NDE.[27–31]

In this Letter, the attenuation characteristics of ZGV Lamb modes, as well as their frequencies, were used quantitatively to distinguish between strongly and weakly bonded samples. Laser ultrasonic measurements were made of five asymmetric trilayer assemblies (aluminum alloy/epoxy/aluminum alloy) with different mechanical strengths. The samples were clearly discriminated thanks to the frequency and the attenuation of the ZGV modes. Quantitative metrics were obtained from the attenuation characteristics, paving the way for a local quantified assessment of the practical adhesion using a contactless nondestructive method.

For a thin elastic plate with two parallel free surfaces, Lamb waves can propagate and are polarized in the sagittal plane.[32] There are symmetrical and anti-symmetrical modes, which are the solutions of the Rayleigh–Lamb equations. These propagation modes are represented in the $\omega - k$ space by dispersion curves, where ω is the angular frequency and k the wavenumber. In particular, ZGV Lamb modes occur when the group velocity vanishes (i.e., $d\omega/dk = 0$) for a finite value of $k \neq 0$. In this case, the energy is locally trapped under the ultrasonic source. A ZGV mode, therefore, behaves as a sharp local resonance of the plate at a well-defined frequency.

For two elastic plates mechanically coupled through an adhesive layer, ZGV modes may also occur and are strongly influenced by the mechanical strength of the coupling. Simulations of the dispersion curves have been used to observe the frequencies of the ZGV modes, which are referred to as ZGV frequencies in the following. When the acoustic wavelength is large compared to the adhesive thickness,[33–35] a bilayer model can be used to represent the bonded assembly [Fig. 1(a)]. In our case, both plates are considered to be homogeneous and isotropic. h_1 is the thickness of the thinner plate and h_2 the thickness of the thicker one. The bonded joint is modeled by normal (K_N) and transverse (K_T) interfacial stiffnesses per unit area.

The dispersion curves were obtained numerically [Fig. 1(b)] for two different cases, based on the approach of Jones and Whittier.[33] First, the top aluminum alloy plate Al_1 with thickness h_1 is considered alone, i.e., $K_N = K_T = 0$ kN mm^{-3}. Symmetrical and anti-symmetrical modes are plotted as dashed and dashed dotted lines, respectively, in Fig. 1(b). Between 0 and 3 MHz, a unique ZGV mode occurs at a frequency of 1.96 MHz, as indicated by the white triangle. Second, coupling between the two plates is imposed by choosing $K_N = K_T = 10$ kN mm^{-3}. The dispersion curves are represented as red solid lines in Fig. 1(b). In this example, there are more guided modes and ZGV modes (shown by red inverted triangles) in the bilayer assembly than for the single plate. Therefore, the theory predicts that, with the higher interfacial stiffnesses, there will be several ZGV modes with similar frequencies due to this mechanical coupling. As a result and as already shown theoretically and experimentally in Ref. 26, any change in the mechanical coupling between the two plates will lead to a modification of the dispersion curves and hence of the ZGV resonance frequencies. Here, we experimentally investigate this ZGV feature for five different bonded samples by analyzing the attenuation of the ZGV modes as a function of time. The samples are now introduced.

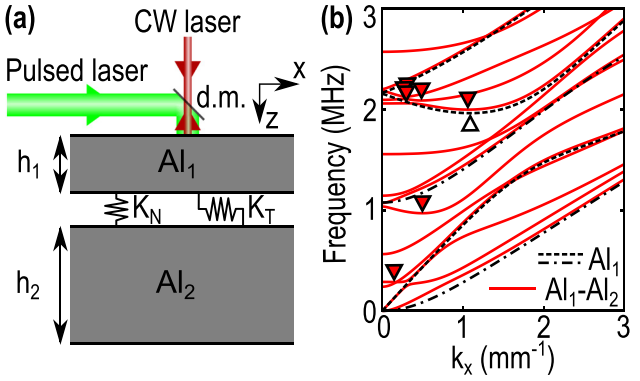

FIG. 1. (a) Schematic diagram of the generation and detection laser paths and of the bilayer model used to simulate the dispersion curves. d.m.: dichroic mirror. K_N, K_T: the normal and transverse interfacial stiffnesses per unit area. (b) The dispersion curves of the top aluminum alloy plate alone (Al_1) are represented as dashed and dashed dotted lines for symmetrical and anti-symmetrical Lamb modes, respectively. The dispersion curves obtained for mechanical coupling between Al_1 and Al_2, with $K_N = K_T = 10$ kN mm^{-3}, are represented as solid lines. ZGV resonances are indicated by white and red triangles.

The first specimen, Al_1, was a 6061 aluminum alloy plate (GoodFellow, United Kingdom), 1.5 mm-thick, and of lateral dimensions 150×150 mm^2. All the other samples were composed of two 6061 aluminum alloy plates, 1.5 mm and 3.0 mm-thick. These plates, of lateral dimensions similar to those of Al_1, were bonded with a structural adhesive film AF 191 (3M^{TM,} United States). During manufacturing, the surfaces of the aluminum alloy plates were first degreased with ethanol. Next, strips of material about 5 mm-wide were placed on the edges of the surfaces, between the two plates, to control the thickness of the epoxy layer (equal to 150 μm) and to prevent the glue from leaking during curing. Then, 16 spring clamps calibrated at 65 N were homogeneously distributed around the sample to maintain a constant pressure during curing.[6] In the nominal case, the bonded sample (subsequently referred to as Nom) was fully cured at 150° C for 3 h.

To simulate cohesive and adhesive defects,[36] two kinds of degradation were implemented. The first was the reduction of the curing time by 50% to lower the cohesive strength of the adhesive. This half-cured sample is labeled C.$_{50}$%. The other type of degradation was the application, with a clean lint-free cloth, of one layer of release agent (R.A.) [Frekote® 44-NC^{TM} (Henkel, Germany)] to a degreased aluminum alloy surface. This layer of release agent disrupted the practical adhesion between the substrate and the fully cured adhesive. The two parts did not become detached, but the structural mechanical strength of the interface of the bonding is significantly reduced using such a protocol. Three samples were produced with this adhesive defect. The first, R.A.$_1$, had one layer of release agent between the first (thin) aluminum plate and the epoxy layer. The second, R.A.$_2$, had the release agent at the interface between the adhesive and the second (thick) aluminum plate. For the third, R.A.$_{1-2}$, both aluminum plates were coated with one layer of Frekote, which affected both interfaces (Table I). All the

bonded samples (except the half-cured sample, C.$_{50\%}$) were cured simultaneously in a laboratory oven at 150° C for 3 h with ramps up and down (heating and cooling) of 2° C min^{-1}. C.$_{50\%}$ was cured at 125 °C for 1.5 h with the same ramps up and down. The longitudinal static strengths were measured to be of the order of 20 MPa for the nominal bonding and 10 MPa (2 MPa) for a sample with cohesive (adhesive) defects. The specimens were indistinguishable in conventional immersion ultrasonic measurements in reflection at 15 MHz.

For the evaluation of these five bonded samples, a laser ultrasonic set-up was used [Fig. 1(a)]. To excite ZGV Lamb modes, a Q-switched Nd:YAG laser (InnoLas Laser GmbH, Germany, SpitLight Compact 400, 532 nm) delivered 8 ns pulses of 200 mJ, with a repetition rate of 10 Hz. To remain in the thermo-elastic (nondestructive) regime, the pump beam was attenuated and then focused onto the surface of the thinnest aluminum plate of the bonded samples. The beam diameter was adjusted to maximize the amplitude of the S_1S_2-ZGV resonance, with the full width at half maximum of the excitation spot approximately equal to half the wavelength of the S_1S_2-ZGV mode[27] of the thin plate. The normal displacement of the surface was measured with a two-wave mixing interferometer (Tecnar, Canada, TWM Laser Ultrasound Detector, 1064 nm, bandwidth 0.7–40 MHz).

For each sample, the generation and the detection laser spots were superimposed [Fig. 1(a)] and swept onto 11 positions with a 1 mm-step in the x-direction. For each measurement point, 500 temporal signals were averaged to increase the signal-to-noise ratio. The fast Fourier transform algorithm was used to process these time-domain signals (Fig. 2). These frequency spectra are normalized with respect to the maximum amplitude of the S_1S_2-ZGV resonance, around 2 MHz, of the 1.5 mm-thick aluminum alloy plate. Since the measurements are reproducible over the 11 positions of the scans (the standard deviations of the measured ZGV frequencies are equal to 1 kHz), only one spectrum per sample is plotted in Fig. 2 for clarity. In the range 0–8 MHz, there are three main peaks around 2, 3, and 6 MHz. Near 3 and 6 MHz, resonance frequencies are visible only for the Al$_1$ and R.A.$_{1-2}$ samples (the orange solid line with square markers and the brown loosely dashed dotted line, respectively). Thanks to the theoretical dispersion curves, the resonance at ∼3 MHz is identified as a thickness mode of the 1.5 mm-thick plate and the one at ∼6 MHz with the S_3S_6-ZGV mode of the 1.5 mm-thick plate. At ∼2 MHz, all the samples have similar but different ZGV frequencies, as can be seen from the inset in Fig. 2. The maximum amplitudes of the peaks also depend on the curing time of the adhesive and on the release agent between the interfaces. Furthermore, notice that for the nominal bonded sample (black solid line labeled Nom), there is no sharp unique ZGV peak, rather two very close resonance frequencies, as identified theoretically. We discuss later why this observation can be extended to R.A.$_1$, C.$_{50\%}$, and R.A.$_2$.

TABLE I. Properties of the samples and fitted values for the attenuation. The bars indicate averages for 11 measurement points. σ is the standard deviation.

	Al$_1$	R.A.$_{1-2}$	R.A.$_1$	C.$_{50\%}$	R.A.$_2$	Nom
Adhesive curing	…	✓	✓	50%	✓	✓
Interface 1[a]	…	Frekote	Frekote	✓	✓	✓
Interface 2[b]	…	Frekote	✓	✓	Frekote	✓
$\overline{G_0}$ (mm μs$^{1/2}$)	0.025	0.012	0.009	0.013	0.012	0.013
$\sigma/\overline{G_0}$ (%)	3%	5%	7%	4%	8%	7%
$\overline{\tau_1}$ (μs)	840	960	102	85	87	63
$\sigma/\overline{\tau_1}$ (%)	23%	7%	17%	27%	34%	23%
$\overline{\delta\omega}/(2\pi)$ (kHz)	0.5	0.5	2.1	6.4	6.8	7.7
$\sigma/\overline{\delta\omega}$ (%)	96%	92%	56%	7%	9%	4%
$\overline{\omega_m}/(2\pi)$ (MHz)	1.964	1.962	2.010	1.992	2.002	1.998
$\sigma/\overline{\omega_m}$ (%)	<0.1%	<0.1%	<0.1%	<0.1%	<0.1%	<0.1%
$\overline{\mathrm{RMSE}}$ (10^{-3})[c]	0.7	0.3	0.2	0.3	0.3	0.4

[a]Interface 1: aluminum alloy plate Al$_1$ (1.5 mm-thick)/adhesive layer.
[b]Interface 2: adhesive layer/aluminum alloy plate Al$_2$ (3.0 mm-thick).
[c]Root-mean square error of the fit.

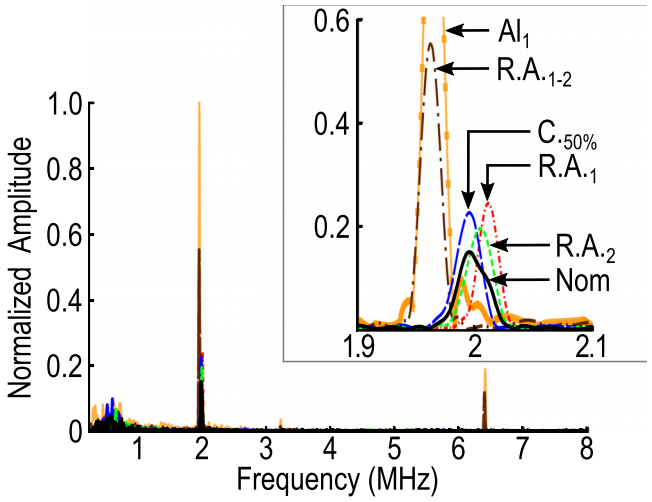

FIG. 2. Experimental frequency spectra in the range 0–8 MHz and around 2 MHz (inset).

The damping of these local resonances provides sufficient information for discriminating the differently prepared samples. The magnitudes of the ZGV modes as a function of time (to a logarithmic scale) are shown in Fig. 3(a). These curves were obtained after filtering the temporal signals with a bandpass filter (Butterworth, order 4, lower and higher cutoff frequencies of 1.5 MHz and 2.5 MHz, respectively) around the ZGV frequency. This filter was chosen for its flat magnitude response in the bandwidth of interest. Typical filtered signals are plotted in Fig. 3(b) for the aluminum alloy plate and for the nominal bonded sample. Then, signal envelopes were extracted with the Hilbert transform, and their magnitudes are displayed in decibels. For each sample, the average attenuation for the 11 measurement points is plotted and the standard deviation is represented with shaded error bars in Fig. 3(a). For the aluminum alloy plate, the S_1S_2-ZGV resonance decreases as a function of $t^{-1/2}$, which agrees with the results of Prada *et al.*,[37] who analytically derived this power law decay,

$$u(t) = G_0 t^{-1/2} e^{-t/\tau_1} \cos(\omega_0 t + \phi), \quad (1)$$

where $u(t)$ is the normal displacement of the surface at the center of the generation laser spot. G_0 is related to the efficiency of the laser-ultrasound generation. It depends on several parameters that are described in Ref. 37, especially the Fourier transform of the spatial and

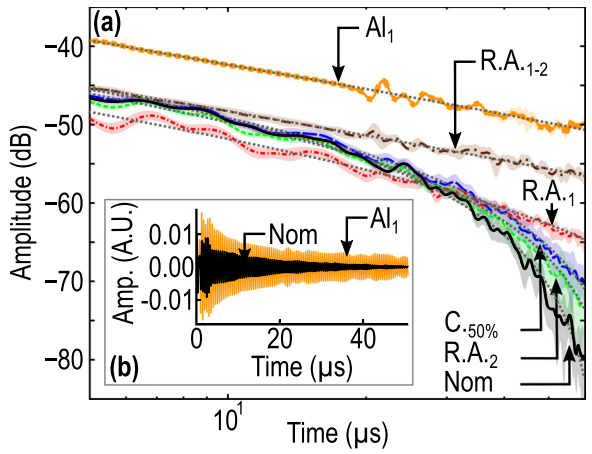

FIG. 3. (a) Experimental attenuation as a function of time to a logarithmic scale. For each sample, the average attenuation for the 11 measurement points is plotted and the standard deviation is represented with shaded error bars. The fitting lines with Eq. (2) are represented with dotted lines. (b) Temporal signals acquired from the aluminum alloy plate and from the nominal bonded sample after filtering the data with a bandpass filter around the ZGV frequency at ∼2 MHz.

temporal profiles of the laser pulse. ω_0 and ϕ are the ZGV angular frequency and the phase, respectively. The time constant τ_1 is for viscoelastic losses, which lead to the exponential decay of the amplitude. For the aluminum alloy plate, this parameter is large ($\overline{\tau_1} = 840$ μs; Table I) so that attenuation is mainly due to the $t^{-1/2}$ factor. As explained by Prada *et al.*,[37] this power law decay is due to the energy that is not trapped under the source, which can, thus, propagate at non-zero group velocity in the medium.

When this model is used to fit the other experimental curves, there are some discrepancies, notably for the bonded samples R.A.$_1$, C.$_{50}$%, R.A.$_2$, and Nom. To address this issue, an additional term is proposed for Eq. (1). It is based on the previous theoretical and experimental observations that the resonance is due to two or more ZGV modes [Fig. 1(b) and the inset of Fig. 2], particularly the black solid curve for the nominal bonded sample. We consider here that the attenuation is due to a beating phenomenon between two close resonances. Assuming that the frequencies have the same phase and amplitude but different frequencies, ω_1 and ω_2, their sum is equivalent to an oscillating signal modulated in amplitude by a cosine function. The angular frequency of the oscillating signal (ω_m) is the mean of ω_1 and ω_2, and the decreasing term is the cosine function, which depends on the slight difference between the frequencies $\delta\omega = \omega_2 - \omega_1$. Therefore, we have

$$u(t) = G_0 t^{-1/2} e^{-t/\tau_1} \cos\left(\frac{\delta\omega t}{2}\right) \cos\left(\omega_m t + \phi\right). \quad (2)$$

The fits of the experimental data with this formula, based on a least squares minimization method, are represented by the dotted lines in Fig. 3(a). There is a relatively good agreement [see the root mean square error (RMSE) of the fits in Table I].

For each sample, the average values and the standard deviations of the metrics G_0, τ_1, $\delta\omega$, and ω_m for the 11 measurement points are listed in Table I. The RMSEs of the fit obtained with Eqs. (1) and (2) are similar for Al$_1$ and R.A.$_{1-2}$. However, the RMSE is higher when the experimental attenuation is fitted with Eq. (1) rather than with Eq. (2). For instance, the RMSE increases by +1%, +27%, +35%, and +42%, respectively, for R.A.$_1$, C.$_{50}$%, R.A.$_2$, and Nom when Eq. (1) is used instead of Eq. (2). Thus, the experimental attenuation is fitted with Eq. (2).

To discriminate between the different samples, the metrics τ_1 and $\delta\omega$ are considered because of their significant sensitivity to bond defects. For the Al$_1$ and R.A.$_{1-2}$ samples, the attenuation is mainly due to the power law decay $t^{-1/2}$. Moreover, note that when Frekote is applied on both sides, the assembly behaves as a freestanding plate. For the samples R.A.$_1$, C.$_{50}$%, R.A.$_2$, and Nom, the decrease in the amplitude as a function of time is also due to viscoelastic losses, with the time constant τ_1, and to the beating phenomenon, with the parameter $\delta\omega$. The Nom sample has the lowest τ_1 (i.e., viscoelastic losses play a major role) and the highest $\delta\omega$ (i.e., the beating phenomenon has a large influence on the attenuation).

Although interface 1 is coated with Frekote for both R.A.$_1$ and R.A.$_{1-2}$, they have different attenuation profiles. This may be because the layer of the release agent does not detach the substrate from the adhesive. The two parts are still mechanically coupled, even if this coupling is weak compared to the nominal case. For R.A.$_1$, only one interface is degraded, while for R.A.$_{1-2}$, two interfaces are degraded. The amount of release agent for R.A.$_{1-2}$ was twice as high as that for R.A.$_1$. This may explain why R.A.$_{1-2}$ behaves more like the top Al$_1$ plate alone than R.A.$_1$.

Thus, the attenuation characteristics in Fig. 3 combined with this identification method allow us to distinguish the different bonded samples and to determine the key metric values that provide a quantification of these differences.

The method was finally tested on a trilayer assembly with two adhesive defects. It had four 75×75 mm^2 zones: two without defects (denominated as previously Nom), one with an adhesive defect R.A.$_1$, and another with R.A.$_2$. 2D maps were produced for the ZGV frequency and attenuation over an area of 80×48 mm^2, which covers the four regions. In Fig. 4(a), the frequency ω_m is plotted vs position. There is clearly no distinct zone with different frequencies, as may be expected. Rather, ω_m changes continuously across the four regions. These interesting monotonous variations show that the effects of a localized adhesive defect spread away from the defect zone. In contrast, τ_1 [Fig. 4(b)] and $\delta\omega$ [Fig. 4(c)] vary non-monotonously across the four regions. The centers of the Nom areas have the highest $\delta\omega$ (as encountered previously; Table I). Assuming, as for the homogeneous samples, that $\delta\omega$ is high where the bonding is actually nominal, Fig. 4(c), thus, shows that the Nom zones are not homogeneous, which strengthens our hypothesis that the effect of a limited adhesive defect is hardly local. Surprisingly, τ_1 is not the lowest in these parts of the Nom areas where $\delta\omega$ is high, which is in contrast with the results in Table I. Note also that a peak is observed in the spectra at ∼1.9 MHz [Fig. 4(d)], which is absent for the homogeneous samples. This peak gives rise to the beating phenomenon [Fig. 4(e)] for a larger $\delta\omega$ than assumed for the minimization.

Two possible reasons may explain why the effects of a localized adhesive defect spread away from its initial deposition area. First, the release agent could migrate from its initial deposition area during curing. This could explain why a continuous change of the ZGV resonance frequency is observed in Fig. 4(a). Second, the differences in the

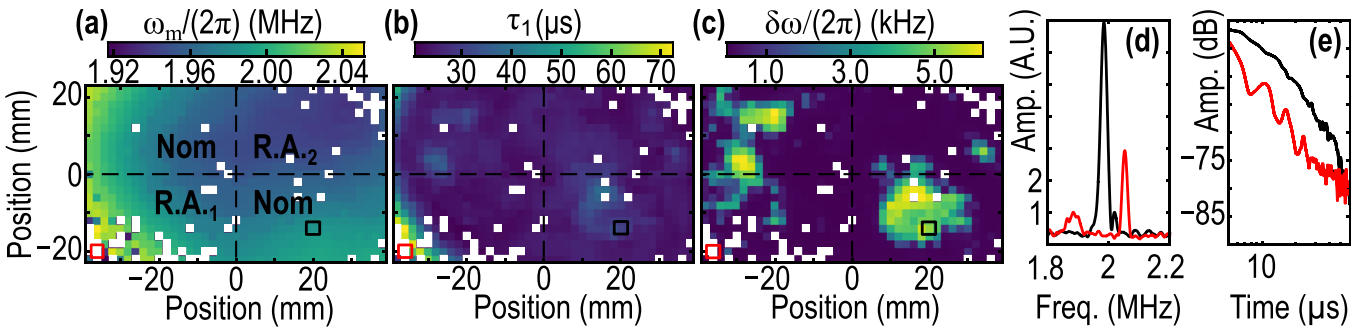

FIG. 4. 2D maps of the metrics of the trilayer sample split into four zones: (a) ω_m, (b) τ_1, and (c) $\delta\omega$. When the RMSE of a fit is higher than 0.4×10^{-3} (maximum value of the previous results for the bonded samples; Table I), the point is rejected and replaced by a white square. (d) Frequency spectra and (e) attenuation of the signals for the red and black boxes in the maps.

practical adhesion in the four areas could lead to residual stresses in the inhomogeneous sample. Therefore, a localized adhesive defect could affect a wider area. Although these unexpected results remain to be explained fully, the metrics τ_1 and $\delta\omega$ have undoubtedly enabled the nondestructive imaging of adhesive bonds with inhomogeneously distributed defects.

We have proposed a laser-based method for generating and detecting ZGV modes so that we can evaluate trilayer assemblies with both cohesive and adhesive defects. By studying the attenuation of ZGV resonances, we have been able to discriminate the different samples thanks to the determination of quantitative metrics (τ_1 and $\delta\omega$). Finally, the imaging ability of this contactless method has been demonstrated with a bonded sample with and without adhesive defects. The root causes of the differences in our results for homogeneously and inhomogeneously distributed defects are now actively under investigation since understanding these could pave the way for quantitative assessments of adhesive bonding using this nondestructive all-optical technique. Laser ultrasonic methods that use non-linear interactions[38,39] could be a valuable approach to improving further the imaging of adhesive bonds.

REFERENCES

[1]C. C. H. Guyott, P. Cawley, and R. D. Adams, J. Adhesion **20**, 129 (1986).
[2]R. D. Adams and B. W. Drinkwater, NDTE Int. **30**, 93 (1997).
[3]B. Ehrhart, B. Valeske, and C. Bockenheimer, "Non-destructive evaluation (NDE) of aerospace composites: Methods for testing adhesively bonded composites," *Non-Destructive Evaluation (NDE) of Polymer Matrix Composites* (Elsevier, 2013), pp. 220–237.
[4]M. D. Bode, M. J. Holle, and D. Westlund, "Literature review of weak adhesive bond fabrication and nondestructive inspection for strength measurement," Technical Report No. DOT/FAA/TC-14/39 (U.S. Departement of Transportation, Federal Aviation Administration, 2015).
[5]L. Berthe, M. Arrigoni, M. Boustie, J. P. Cuq-Lelandais, C. Broussillou, G. Fabre, M. Jeandin, V. Guipont, and M. Nivard, Nondestr. Test. Eval. **26**, 303 (2011).
[6]M. Ducousso, S. Bardy, Y. Rouchausse, T. Bergara, F. Jenson, L. Berthe, L. Videau, and N. Cuvillier, Appl. Phys. Lett. **112**, 111904 (2018).
[7]B. Ehrhart, R. Ecault, F. Touchard, M. Boustie, L. Berthe, C. Bockenheimer, and B. Valeske, Int. J. Adhes. Adhes. **52**, 57 (2014).
[8]H. G. Tattersall, J. Phys. D: Appl. Phys. **6**, 819 (1973).
[9]F. H. Chang, P. L. Flynn, D. E. Gordon, and J. R. Bell, IEEE Trans. Sonics Ultrason. **23**, 334 (1976).
[10]A. Pilarski and J. L. Rose, J. Appl. Phys. **63**, 300 (1988).
[11]A. Baltazar, L. Wang, B. Xie, and S. I. Rokhlin, J. Acoust. Soc. Am. **114**, 1424 (2003).
[12]E. Siryabe, M. Rénier, A. Meziane, J. Galy, and M. Castaings, Ultrasonics **79**, 34 (2017).
[13]W.-L. Wu, X.-G. Wang, Z.-C. Huang, and N.-X. Wu, AIP Adv. **7**, 125316 (2017).
[14]P. Zabbal, G. Ribay, and J. Jumel, AIP Conf. Proc. **2102**, 020030 (2019).
[15]P. B. Nagy and L. Adler, J. Appl. Phys. **66**, 4658 (1989).
[16]R. Seifried, L. J. Jacobs, and J. Qu, NDTE Int. **35**, 317 (2002).
[17]B. L. Crom and M. Castaings, J. Acoust. Soc. Am. **127**, 2220 (2010).
[18]M. Castaings, Ultrasonics **54**, 1760 (2014).
[19]C. Gauthier, M. Ech-Cherif El-Kettani, J. Galy, M. Predoi, and D. Leduc, Int. J. Adhes. Adhes. **98**, 102467 (2020).
[20]C. Prada, O. Balogun, and T. Murray, Appl. Phys. Lett. **87**, 194109 (2005).
[21]D. Clorennec, C. Prada, and D. Royer, IEEE Trans. Ultrason., Ferroelectr., Freq. Control **57**, 1125 (2010).
[22]H. Cho, Y. Hara, and T. Matsuo, J. Phys.: Conf. Ser. **520**, 012023 (2014).
[23]S. Mezil, J. Laurent, D. Royer, and C. Prada, Appl. Phys. Lett. **105**, 021605 (2014).
[24]H. Cho, Y. Yaguchi, and H. Ito, Mech. Eng. J. **2**, 14-00335 (2015).
[25]S. Dahmen, Ultrasonics **94**, 37 (2019).
[26]S. Mezil, F. Bruno, S. Raetz, J. Laurent, D. Royer, and C. Prada, J. Acoust. Soc. Am. **138**, 3202 (2015).
[27]O. Balogun, T. W. Murray, and C. Prada, J. Appl. Phys. **102**, 064914 (2007).
[28]C. Grünsteidl, T. W. Murray, T. Berer, and I. A. Veres, Ultrasonics **65**, 1 (2016).
[29]F. Faëse, S. Raetz, N. Chigarev, C. Mechri, J. Blondeau, B. Campagne, V. E. Gusev, and V. Tournat, NDTE Int. **85**, 13 (2017).
[30]C. Grünsteidl, T. Berer, M. Hettich, and I. Veres, Appl. Phys. Lett. **112**, 251905 (2018).
[31]G. Yan, S. Raetz, N. Chigarev, V. E. Gusev, and V. Tournat, Phys. Rev. Appl. **9**, 061001 (2018).
[32]D. Royer and E. Dieulesaint, *Elastic Waves in Solids I: Free and Guided Propagation* (Springer Berlin Heidelberg, 1999).
[33]J. P. Jones and J. S. Whittier, J. Appl. Mech. **34**, 905 (1967).
[34]S. I. Rokhlin and Y. J. Wang, J. Acoust. Soc. Am. **89**, 503 (1991).
[35]V. Vlasie and M. Rousseau, Wave Motion **37**, 333 (2003).
[36]D. Jiao and J. L. Rose, J. Adhes. Sci. Technol. **5**, 631 (1991).
[37]C. Prada, D. Clorennec, and D. Royer, Wave Motion **45**, 723 (2008).
[38]C.-Y. Ni, N. Chigarev, V. Tournat, N. Delorme, Z.-H. Shen, and V. E. Gusev, J. Acoust. Soc. Am. **131**, EL250 (2012).
[39]S. Mezil, N. Chigarev, V. Tournat, and V. Gusev, Ultrasonics **69**, 225 (2016).